Chemical Engineering Journal 421 (2021) 127734

Contents lists available at ScienceDirect

Chemical Engineering Journal

journal homepage: www.elsevier.com/locate/cej

High-purity nitrogen production from air by pressure swing adsorption combined with $SrFeO_3$ redox chemical looping☆

B. Bulfin *, L. Buttsworth, A. Lidor, A. Steinfeld

Department of Mechanical and Process Engineering, ETH Zürich, 8092 Zürich, Switzerland

ARTICLE INFO

Keywords:
Nitrogen production
Oxygen separation
Pressure swing adsorption
Redox cycle
Chemical looping

ABSTRACT

The combination of pressure swing adsorption (PSA) with a downstream redox chemical looping cycle to remove trace oxygen is proposed for the production of high-purity nitrogen from atmospheric air. The non-stoichiometric perovskite $SrFeO_{3-\delta}$ is selected for the redox chemical looping cycle because of its favourable thermodynamics, rapid oxidation kinetics and intermediate reduction temperatures. Long term stability of the material was demonstrated over 250 redox cycles via thermogravimetry. Oxidation kinetics were measured and incorporated in a 1D convection–diffusion model of a packed bed reactor configuration. The model indicates that, for a targeted oxygen impurity level of $x_{O_2} < 3 \times 10^{-6}$, a chemical looping unit added to a PSA system could approximately triple the capacity and reduce the energy demand to $14 kJmol^{-1}$ of N_2.

1. Introduction

Nitrogen makes up 78% of the earth's atmosphere. Its triple bond N≡N is extremely stable, making the gas inert under most circumstances. Despite this chemical stability, natural fixation of nitrogen from the atmosphere and its subsequent chemical reactions are vital for the biosphere, with these processes known collectively as the biogeochemical nitrogen cycle. Indeed, the fixation of nitrogen is often the bottle-neck that limits growth rate for many plants, including domesticated species. In the early 20th century, the Haber–Bosch process was commercialised, offering a synthetic route to nitrogen fixation via ammonia production. This would lead to an ever increasing demand for nitrogen, with ammonia among the world's most produced chemicals using as much as 1% of global primary energy [1].

Different applications of nitrogen require different purities and production capacities. Fig. 1 shows capacity vs. purity trends for some of the larger scale units commercially available, including; fractional distillation of cryogenic liquefied air, pressure swing adsorption (PSA), and membrane separation units. Each of these technologies use mechanical compression as the source of work that powers the separation of nitrogen from air, but the processes after compression are quite different [2]. In a cryogenic plant, moisture and CO_2 are first removed from the compressed air, before volumetric expansion and a series of very effective heat exchangers are used to cool the air until it condenses. The liquid air is then passed to a distillation column, offering a very pure stream of nitrogen from the top of the distillation column [2].

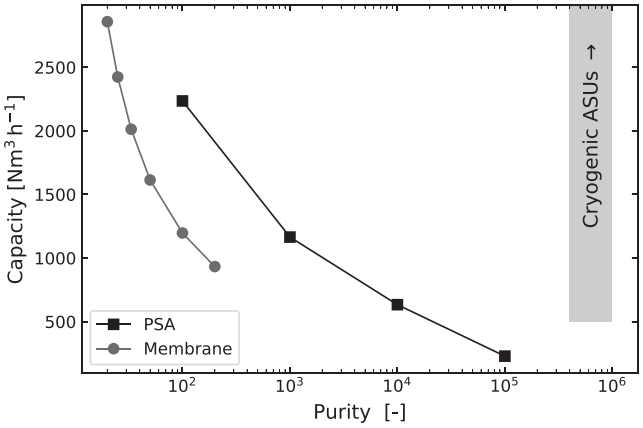

Fig. 1. Production capacity vs. nitrogen purity $\left(\frac{1}{x_{O_2}}\right)$ for commercially available nitrogen production units. Data from gas separation company Genron, is shown for membrane (model 6830CP) and PSA (model NS-60-94) systems, which are some of the larger scale units commercially available. For cryogenic air separation units (ASUs), companies Linde and Cryogenmash offer systems ranging from 500–8000+ [N m^3 h^{-1}].

In a PSA system the compressed air is passed through a packed bed of adsorption material, e.g. a carbon molecular sieve, which adsorb O_2,

☆ Electronic Supplementary Information (ESI) available.

* Corresponding author.
E-mail address: bulfinb@ethz.ch.ch (B. Bulfin).

https://doi.org/10.1016/j.cej.2020.127734
Received 22 September 2020; Received in revised form 9 November 2020; Accepted 12 November 2020
Available online 17 November 2020

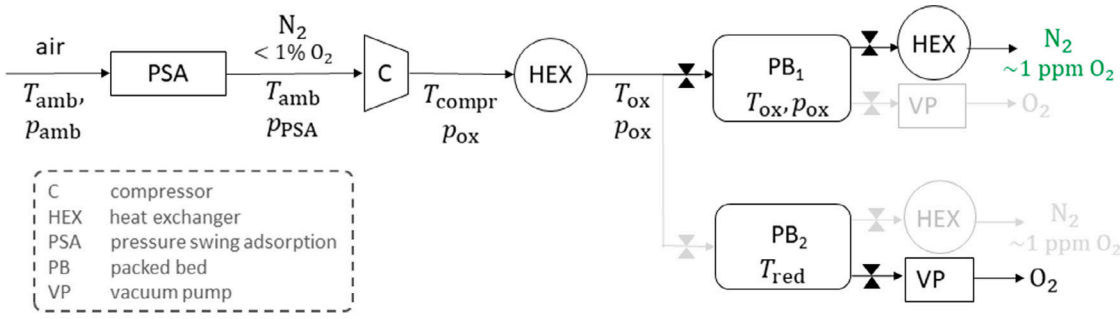

Fig. 2. A schematic of the proposed process chain. Nitrogen is first separated from air via PSA, compressed and then passed through a packed bed of reduced $SrFeO_3$ to remove residual oxygen. The two packed bed reactors then alternate between oxidation for gas purification, and reduction for regeneration of the bed.

H_2O, and CO_2 more readily than N_2 [2,3]. Purified N_2 exits the packed bed, which is periodically regenerated by releasing the pressure to desorb the gases (and pumping it down to vacuum pressures), with two packed beds required for continuous operation. In a membrane system the gas is passed through a large array of hollow fibres which more readily permeate O_2, H_2O, and CO_2 [2], so that more concentrated nitrogen exits the end of the fibres.

Generally, the life-cycle cost normalised per mole of nitrogen, increases with purity and decrease with scale. Cryogenic systems require the expansion, heat exchangers and low temperature distillation to be performed in an insulated cold-box, increasing the plant complexity relative to a PSA system [2]. The energy demand of the compressors and effectiveness of the heat-exchangers benefit greatly by scaling up the system. Although intermediate scale cryogenic plants are available at 500 N $m^3\,h^{-1}$, manufacturers data indicates that they have double the power demand of large scale systems (from Cryogenmash). On the other hand, the capacity of a PSA unit decreases significantly with increasing purity (see Fig. 1), while the installation cost and power demand remain approximately the same. This is because the PSA packed beds need to be regenerated much more frequently to maintain the high purity.

It can also be seen from Fig. 1, that for purities in the range 10^3–10^5 and capacities above 800 N $m^3\,h^{-1}$, that neither PSA nor membrane technologies are well suited. Applications in this region may be forced to opt for a more expensive cryogenic system. An interesting option to upgrade the purity of the nitrogen from a PSA system without drastically decreasing the capacity, is to add a deoxygenation (deoxo) step to the process [3]. This is downstream of the PSA, and uses chemical reactions to directly remove oxygen. In the past a chemical looping of copper oxide has been employed [3],

$$O_2(g) + 2Cu(s) \longrightarrow 2CuO(s), \tag{1}$$

which is regenerated using hydrogen,

$$CuO(s) + H_2(g) \longrightarrow Cu(s) + H_2O(g). \tag{2}$$

This allowed PSA systems to achieve higher purity and maintain a larger capacity. However, this is a rather complex add on unit which requires H_2 for regeneration, and as noted by Shulte et al., this results in a large cost increase for the system [3].

In this work we propose another deoxygenation route using a chemical looping cycle of non-stoichiometric $SrFeO_3$,

$$SrFeO_3 \xleftrightarrow{\delta(T,p_{O_2})} SrFeO_{3-\delta} + \frac{\delta}{2} O_2. \tag{3}$$

This material can be regenerated using a temperature and pressure swing cycle as opposed to hydrogen [4]. It has been extensively studied for its non-stoichiometric redox properties [5,6], and its potential for application in air separation [7,8]. Many other materials including manganese and cobalt based perovskites, have also recently been suggested for air separation processes [9–11], but $SrFeO_{3-\delta}$ was chosen for the balance it strikes between ease of reduction, its relatively strong oxygen affinity, and its rapid oxidation kinetics at temperatures in the range 500–650 K [4,12].

Fig. 2 shows a schematic of the proposed PSA-deoxo process, where roughly purified nitrogen from a PSA system ($x_{O_2} < 0.01$) is further purified using packed beds of reduced $SrFeO_{3-\delta}$ to remove oxygen to ppm levels. In this work we set a cut-off oxygen impurity of 3 ppm, so that this is the maximum oxygen fraction in the gas leaving the process, which has been demonstrated at lab-scale [4]. The deoxo unit consists of a heat exchanger, two packed beds and a vacuum pump. While the oxidation of one $SrFeO_{3-\delta}$ packed bed is absorbing oxygen from the stream at $T_{ox} \approx 600$ K, the other bed is being regenerated by heating to $T_{red} \approx 850$ K and reducing the $SrFeO_3$ with a vacuum pump to remove additional oxygen at low partial pressures. The nitrogen coming from the PSA system is usually at 7–10 bar, which can be further compressed (optional) before the deoxo system, as this can improve the amount of oxygen absorbed per cycle in the packed beds. If the nitrogen is required at higher pressures than 7–10 bar, the compression before the deoxo unit would come at no extra cost as the gas would need to be compressed either way.

In this work we analyse the technical feasibility and potential performance of this process. We start with a first principles thermodynamic analysis to determine the energy demand relative to a PSA system alone. We then perform an experimental analysis of oxidation kinetics and chemical stability of $SrFeO_3$, both at the conditions relevant for the process (see Table 1). In total we performed 250 cycles of $SrFeO_{3-\delta}$ redox chemical looping at the suggested process temperatures to demonstrate its high chemical stability. We formulate a kinetic model of a single pellet, which can be used to model the packed beds. The packed beds of $SrFeO_{3-\delta}$ are one of the main components of the process, and the only part which is not yet fully developed. Therefore, to assess this component we develop a 1D convection–diffusion model with a chemical source term based on the kinetic model. We validate the model for a demonstration experiment [4]. Finally, a scaled up system for the production of 1000 N m^{-3} h^{-1} of nitrogen with an oxygen impurity $x_{O_2} < 3e{-}6$ is modelled.

2. Thermodynamic model

In this section we develop a first principles thermodynamic model of the process illustrated in Fig. 2, which should allow us to determine the energy demand of the process. To perform this energy balance we break the process into a number of separate steps. First the air enters the PSA unit, where CO_2, H_2O and O_2 are removed, with oxygen remaining at a mole fraction $x_{O_2,PSA}$, e.g. 1%. This requires a work input W_{PSA}. The gas stream leaving the PSA at a pressure of 7 bar [13] can then be further compressed, which requires a work input W_{compr}. The gases then need to be heated up to the oxidation temperature requiring a heat input Q_{gas}. A heat exchanger can be used between the gas exiting and entering the packed bed to reduce this energy demand.

After passing through the heat exchanger, the gas enters one of the packed beds (PB) containing $SrFeO_3$ (SF) where further oxygen

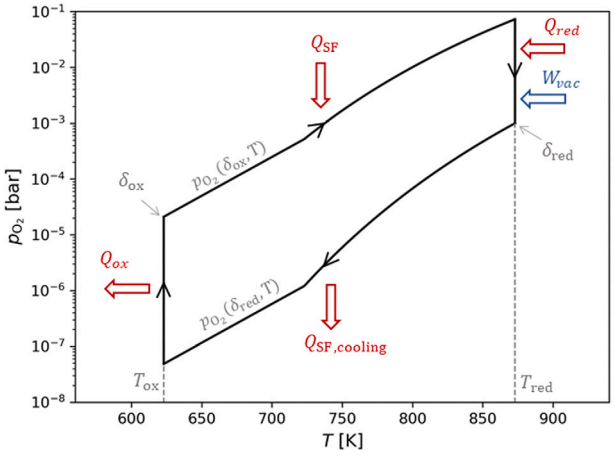

Fig. 3. A $p_{O_2} - T$ diagram of the thermodynamic redox cycle with energy inputs and outputs. The parameters for this cycle are given in Table 1. In the thermodynamic model, the $SrFeO_{3-\delta}$ is always in equilibrium with p_{O_2}. The cycle then takes place between two isotherms, T_{ox} and T_{red}, and two equilibrium contours at constant δ, $p_{O_2}(\delta_{ox},T)$ and $p_{O_2}(\delta_{red},T)$. These equilibrium contours are determined by the redox material $SrFeO_3$.

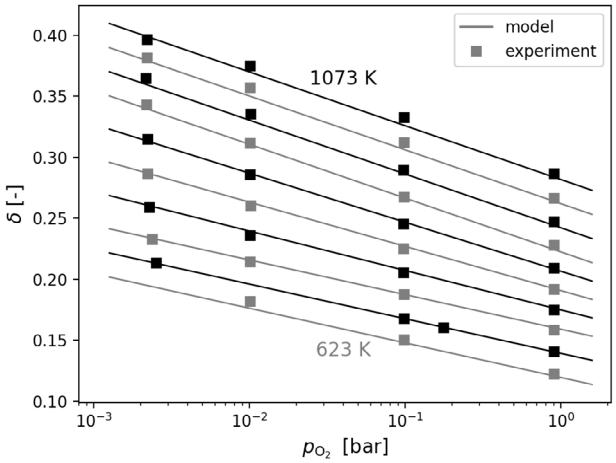

Fig. 4. Equilibrium isotherms of non–stoichiometry δ vs. p_{O_2} for $SrFeO_{3-\delta}$, plotted at temperatures in the range 623-1073 K in steps of 50 K. Squares are experimentally measured values from Bulfin et al. [4], solid lines are values calculated with our $\delta_{eq}(T, p_{O_2})$ model, see ESI Section 1.

is removed, leading to an outlet nitrogen stream with oxygen mole fractions on the order of ppm. In the packed bed the SF undergoes a redox cycle illustrated on a p-T diagram in Fig. 3. During the isothermal oxidation step at T_{ox}, SF takes up oxygen until a non-stoichiometry of δ_{ox}. During the isothermal reduction step at T_{red}, the absorbed oxygen is removed from the packed bed via a reduction reaction leading to a non-stoichiometry of δ_{red}. The energy inputs to this cycle are; the heating up of the SF packed bed during the temperature swing from T_{ox} to T_{red} when switching from oxidation to reduction, Q_{SF}, and the enthalpy change of the endothermic reduction step, Q_{red}. The heat released by the cycle is the cooling down of the packed when changing from the reduction step to the oxidation step, and the reaction enthalpy of the exothermic oxidation. As can be seen in Fig. 2, during the reduction, a vacuum pump is employed, which also requires a work input W_{vac}.

The total energy demand for the process is then given by,

$$E_{tot} = W_{PSA} + W_{compr} + Q_{gas} + Q_{SF} + Q_{red} + W_{vac} \quad (4)$$

For W_{PSA}, W_{compr}, Q_{gas}, and W_{vac} we can use established functions and thermodynamic databases. However, for the redox cycle (Q_{SF} and Q_{red}) we need a consistent thermodynamic model of $SrFeO_3$, as described below.

2.1. $SrFeO_3$ thermodynamics

The perovskite $SrFeO_{3-\delta}$ undergoes non stoichiometric reduction as show in Eq. (3), where the values of δ varies with temperature and the partial pressure of oxygen. Previous investigations of this redox system report equilibrium data for the non-stoichiometry at a wide range of temperature and oxygen partial pressures $\delta_{eq}(T, p_{O_2})$ [5,6,14–17], which was combined with previous work of the authors [4], to formulate an equilibrium model of $SrFeO_3$. It allows for the calculation of equilibrium non-stoichiometry $\delta_{eq}(T, p_{O_2})$, and given δ the equilibrium oxygen partial pressure $p_{O_2,eq}(\delta, T)$. This can be seen in comparison to experimental values from Bulfin et al. [4] in Fig. 4. The details of the model can be found in the ESI Section 1.

The heat capacity of SF was calculated using the elastic tensor (from 0 K DFT) and the Debye Model as described by Vieten et al. [18] and linearly interpreted between the end member reduction states. This results in a heat capacity which depends on both the non-stoichiometry and the temperatures $C_{p,SF}(\delta, T)$, with full details given in the ESI.

The reaction enthalpy change required to reduce $SrFeO_3$ ΔH_{red} was calculated using the value of 65 kJ mol_O^{-1} (per mole of atomic oxygen) reported by Sereda et al. [17] at 923 K, and using Kirchhoff's law to extrapolate to other temperatures. Since the heat capacity of SF has both a T and a δ dependence, this results in an enthalpy of reaction which depends on both temperature, and the start and end point non stoichiometries $\Delta H_{red}(\delta_{initial}, \delta_{final}, T)$. This method of using Kirchhoff's law together with our theoretical heat capacities ensures a closed energy balance for the material around a redox cycle.

2.2. Thermodynamic model assumptions

In order to model the packed bed redox cycle, we make the following assumptions;

1. The temperature, pressure and concentrations are assumed to be constant throughout the packed bed reactors, so that they can be modelled as zero dimensional.
2. The redox reactions only take place at T_{red} and T_{ox}.
3. The oxygen partial pressure is in equilibrium with the $SrFeO_{3-\delta}$ throughout the oxidation step.
4. Residual nitrogen in the reactor at the end of oxidation can be neglected in the vacuum pumping reduction step.
5. The gas coming from the PSA has a constant oxygen impurity $x_{O_{2,PSA}}$, i.e. not varying with time.

The first assumption is equivalent to assuming an ideal perfect mixing flow reactor, which greatly simplifies the model, but also underestimates the performance relative to a plug flow reactor. The second assumption is valid for oxidation, where the reaction cannot take place until the oxidant is introduced at T_{ox}. For reduction, some reduction could take place during the heating up phase, but the assumption conserves the net energy balance and serves to simplify the computation. The third assumption is that the kinetics of the reactions are fast enough to allow the system to come very close to equilibrium at all times during oxidation, which is supported by kinetic analysis of $SrFeO_3$ showing rapid oxidation at the temperature considered [12]. The fourth assumption is justified by a calculation of the relative amount of residual nitrogen and oxygen to be pumped, which is given in the thermodynamic model section of the ESI. The fifth assumption is a simplification, as a detailed model of the PSA system adds a lot of complexity. This assumption could be achieved in practice by using a buffer tank after the PSA system to smooth the oxygen impurity output.

2.3. Energy balance

Here we outline the calculations of the energy demand of each part of the process, in all cases per mole of nitrogen produced. This includes a mass balance of the redox process.

The work of the PSA was calculated with the empirical formula developed by Krenzke et al. in [19] as,

$$W_{\mathrm{PSA}} = \frac{1}{(1 - x_{\mathrm{O_2,PSA}})} \log\left(\frac{x_{\mathrm{O_2},in}}{x_{\mathrm{O_2,PSA}}}\right) \cdot 1000 \quad \left[\mathrm{J\ mol}_{\mathrm{N_2}}^{-1}\right]. \tag{5}$$

where the $x_{\mathrm{O_2,in}} = 0.21$ is the oxygen mole fraction of air, $x_{\mathrm{O_2,PSA}}$ is the mole fraction of oxygen leaving the PSA system. The subscript in the units is to indicate that this is per mole of N_2. The factor of $\frac{1}{(1-x_{\mathrm{O_2,PSA}})}$ accounts for the change in moles after the residual oxygen is removed.

The work to compress the mixture of N_2 and O_2 from the PSA system to the oxidation pressure of the packed bed W_{compr}, was calculated by assuming an 85% efficient adiabatic compressor. The ideal adiabatic compression energy demand was calculated using an isentropic pressure change, for our given gas mixture with cantera [20],

$$W_{\mathrm{compr}} = \frac{1}{0.85(1 - x_{\mathrm{O_2,PSA}})} W_{\mathrm{ideal-adiabatic}}(p_{\mathrm{PSA}}, p_{\mathrm{ox}}) \quad \left[\mathrm{J\ mol}_{\mathrm{N_2}}^{-1}\right] \tag{6}$$

where the 0.85 accounts for the efficiency, and $\frac{1}{(1-x_{\mathrm{O_2,PSA}})}$ accounts for the change in number of moles after removing the oxygen.

The gas heat energy demand was calculated using the formulae,

$$Q_{\mathrm{gas}} = \begin{cases} Q_{\mathrm{gas,in}} + \eta_{\mathrm{HE}} Q_{\mathrm{gas,out}} & Q_{\mathrm{gas,in}} > \eta_{\mathrm{HE}} Q_{\mathrm{gas,out}} \\ 0 & Q_{\mathrm{gas,in}} \leq \eta_{\mathrm{HE}} Q_{\mathrm{gas,in}} \end{cases} \quad [\mathrm{J\ mol}_{\mathrm{N_2}}^{-1}], \tag{7}$$

where $Q_{gas,in}$ and $Q_{\mathrm{gas,out}}$ are the sensible heats of the incoming and outgoing gases respectively. The heat exchanger efficiency was set to a conservative $\eta_{\mathrm{HE}} = 0.8$. To calculate the sensible heat of the gases, the specific heat (taken from NIST Chemistry WebBook) was integrated from T_{amb} to T_{ox}.

To heat the SF up to the reduction temperature we require a heat input,

$$Q_{\mathrm{SF}} = n_{\mathrm{SF}} \int_{T_{ox}}^{T_{red}} C_{p,\mathrm{SF}}(\delta_{\mathrm{ox}}, T)\, dT \quad [\mathrm{J\ mol}_{\mathrm{N_2}}^{-1}], \tag{8}$$

where n_{SF} is number of moles of perovskite which needs to be cycled in order to produce 1 mole of N_2. It has an approximate dependence,

$$n_{\mathrm{SF}} \approx \frac{2x_{\mathrm{O_2,PSA}}}{\Delta\delta} \quad [\mathrm{mol/mol}_{\mathrm{N_2}}], \tag{9}$$

where $\Delta\delta = \delta_{\mathrm{red}} - \delta_{\mathrm{ox}}$. This is the amount of oxygen in the gas coming from the PSA divided by the oxygen storage of the SF $\Delta\delta$. The complete oxygen mass balance between the gas and solid, is given in the ESI.

The energy demand for the reduction of SF, Q_{red}, is given by,

$$Q_{\mathrm{red}} = n_{\mathrm{SF}} \Delta H_{red}(\delta_{\mathrm{ox}}, \delta_{\mathrm{red}}, T_{\mathrm{red}}) \quad [\mathrm{J\ mol}_{\mathrm{N_2}}^{-1}], \tag{10}$$

where the reaction enthalpy $\Delta H_{\mathrm{red}}(\delta_{\mathrm{ox}}, \delta_{\mathrm{red}}, T_{\mathrm{red}})$ calculation is given in Section 1 of the ESI.

During reduction the pressure will be pumped down from atmospheric pressure to remove additional oxygen. The work demand of the vacuum pump is calculated using the formulae,

$$W_{\mathrm{vac}} = n_{\mathrm{SF}} \frac{\delta_{\mathrm{red}} - \delta_{\mathrm{ox}}}{2} \int_{\delta_{\mathrm{ox}}}^{\delta_{\mathrm{red}}} W_{\mathrm{vac.\ pump}}(p_{\mathrm{O_{2,eq}}}(\delta, T_{\mathrm{red}}))\, d\delta \quad [\mathrm{J\ mol}_{\mathrm{N_2}}^{-1}], \tag{11}$$

where we pump along the equilibrium partial pressure contour $p_{\mathrm{O_2}}(\delta, T_{\mathrm{red}})$ and use the model of Brendelberger et al. for the vacuum pump energy demand as a function of pressure $W_{\mathrm{vac.\ pump}}(p)$ [21]. There are also cases where the equilibrium oxygen pressure is greater than atmospheric pressure. In such cases oxygen released above atmospheric pressure was omitted from the W_{vac} integral. For the pressure dependence of the vacuum pump see the ESI.

Table 1
Parameters for the base case of the energy balance.

PSA process		
$x_{\mathrm{O_2,PSA}}$	0.01	[–]
p_{PSA}	7	[bar]
Redox cycle		
T_{ox}	623	[K]
T_{red}	873	[K]
p_{ox}	7	[bar]
p_{red}	0.001	[bar]
$\delta_{\mathrm{ox}} = \delta_{\mathrm{eq}}(x_{\mathrm{O_2,cut-off}} p_{\mathrm{ox}}, T_{\mathrm{ox}})$	0.252	[–]
$\delta_{\mathrm{red}} = \delta_{\mathrm{eq}}(p_{\mathrm{red}}, T_{\mathrm{red}})$	0.327	[–]
$x_{\mathrm{O_2,cut-off}}$	3×10^{-6}	[–]
Energy demand		
E_{tot}	17.5	[kJ $\mathrm{mol}_{\mathrm{N_2}}^{-1}$]
$W_{\mathrm{PSA\ alone}}$	22	[kJ $\mathrm{mol}_{\mathrm{N_2}}^{-1}$]

There is also heat released from the system during the cooling of the packed bed $Q_{\mathrm{SF,cooling}}$ and as a result of the exothermic oxidation reaction Q_{ox}. This released heat is approximately equal to the heat supplied to the redox cycle. Here we simply assume that the this released heat is lost to the ambient.

2.4. Energy balance results

The base case parameters and the total energy demand for the process are given in Table 1. We assume that the operation of the beds is switched whenever the oxygen impurity reaches 3 ppm. This gives us a cut-off mole fraction of $x_{\mathrm{O_2,cutoff}} = 3 \times 10^{-6}$. The parameters of the base case redox cycle were chosen using practical considerations and with the aim of maximising the oxygen storage in the SF, $\Delta\delta$. The oxygen storage $\Delta\delta$, has an inverse relationship with the number of moles of SF, n_{SF} (Eq. (9)), and is crucial for the energy demand (Q_{SF} and Q_{red}) and feasibility of the system. To achieve a large $\Delta\delta$ the reduction temperature T_{red} is significantly higher than the oxidation temperature, but low enough that standard stainless steel could be used for constructing the packed bed. Similarly, a lower reduction pressure p_{red} would increase $\Delta\delta$, but we also need to consider the energy demand and size of the vacuum pump required. A lower oxidation temperature T_{ox} would also increase $\Delta\delta$, but this was not considered as the kinetic activity may be an issue at lower temperatures. Finally, the oxidation pressure was set equal to the pressure of the PSA system $p_{\mathrm{ox}} = p_{\mathrm{PSA}}$, so that the compressor is unused in the base case and $W_{\mathrm{compr}} = 0$.

Also given in Table 1 is the total energy demand of the process with the base case parameters and for comparison, the energy demand of using PSA alone to achieve the same purity level according to the model of Krenzke et al. given in Eq. (5). This shows that the addition of the packed bed redox cycle to remove trace oxygen could improve the energy demand of high purity nitrogen production relative to a PSA system. It also has the benefit that the PSA system can run at lower purity output and thus higher capacity (see Fig. 1).

At this point we can also perform parametric studies around the base case analysis. As mentioned already the number of moles of SF required to be cycled per mole of nitrogen produced, n_{SF}, is a very important parameter for the energy balance. As well as depending on $\Delta\delta$, it is directly proportional to the oxygen impurity level in the gas coming from the PSA $x_{\mathrm{O_2,PSA}}$, as can be seen in Eq. (9). We therefore first look at the effect of $x_{\mathrm{O_2,PSA}}$ on the energy balance. Practically speaking this parameter decides how much of the separation is done by the PSA system before using the redox cycle to upgrade the purity.

With other parameters from the base case fixed, $x_{\mathrm{O_2,PSA}}$ was varied from 3×10^{-6} to 0.02, with the results shown in Fig. 5. Comparing E_{tot} with $W_{\mathrm{PSA,alone}}$, we see that for $x_{\mathrm{O_2,PSA}} > 0.015$ (1.5% oxygen), our process needs more energy than using just the PSA system to achieve the same purity. This is because the SF redox process has a relatively

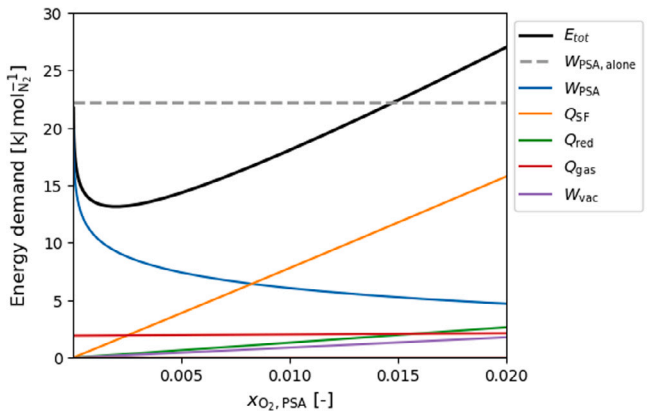

Fig. 5. Total energy demand of the process E_{tot} vs. $x_{O_2,PSA}$. Also plotted is the energy demand required to achieve the same purity using PSA alone $W_{PSA,alone}$ according to Eq. (5), and each contribution to the total energy demand, $E_{tot} = W_{PSA} + Q_{SF} + Q_{red} + Q_{gas} + W_{vac}$.

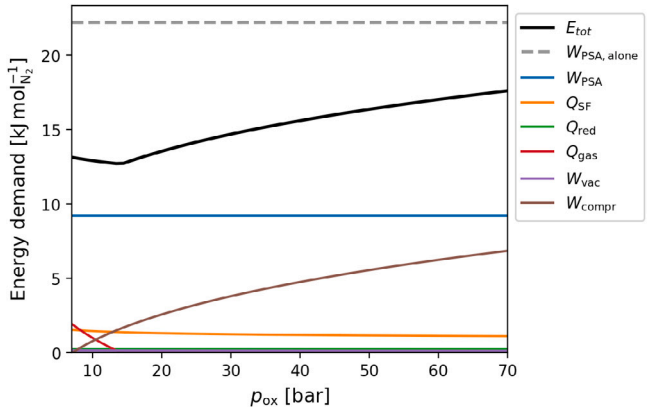

Fig. 6. Total energy demand E_{tot} vs. p_{ox}, with $x_{O_2,PSA} = 0.002$, while the other parameters are those of the base case given in Table 1. Also plotted is the energy demand using PSA alone $W_{PSA,alone}$, and each contribution to the total energy demand, $E_{tot} = W_{PSA} + Q_{SF} + Q_{red} + Q_{gas} + W_{vac} + W_{compr}$.

large energy demand that scales directly with the number of moles of oxygen to be removed. This can be seen by the linear trend Q_{SF} has on $x_{O_2,PSA}$, while the energy demand of the PSA W_{PSA}, has a logarithmic dependence on the purity $x_{O_2,PSA}$. These converse trends lead to E_{tot} showing an optimum at approximately $x_{O_2,PSA} = 0.002$.

The influence of using a compressor after the PSA to increase p_{ox} was studied by varying p_{ox} from 7 bar to 70 bar, with the results shown in Fig. 6. With increasing oxidation pressure p_{ox}, the E_{tot} initially decreases because the higher p_{ox} leads to a more oxidised δ_{ox}, which in turn leads to lower n_{SF} and a lower energy demand for the redox cycle. The heat necessary to heat the gases Q_{gas}, also decreases and becomes zero at $p_{ox} = 15$ bar, because the compression also heats the gases. At this point there is a kink where further compression increases the energy demand. Further compression may negate the need for a heat exchanger, and in the case where the end user requires high pressure nitrogen, it could reduce the cost of the system. Increasing p_{ox} may also have advantages for the performance of the SF packed bed reactors. A higher pressure increases the oxygen concentration C_{O_2} and reduces volumetric flow rates, which increases the residence time.

The other parameters important in deciding $\Delta\delta$ and thus also n_{SF} are the reduction conditions, T_{red} and p_{red}. The results of varying these parameters can be seen in Fig. 7. For each p_{red} there is a steep increase in E_{tot} at some point as we decrease T_{red}. This vertical increase is where δ_{red} approaches δ_{ox} and, thus $\Delta\delta$ approaches zero and n_{SF} approaches

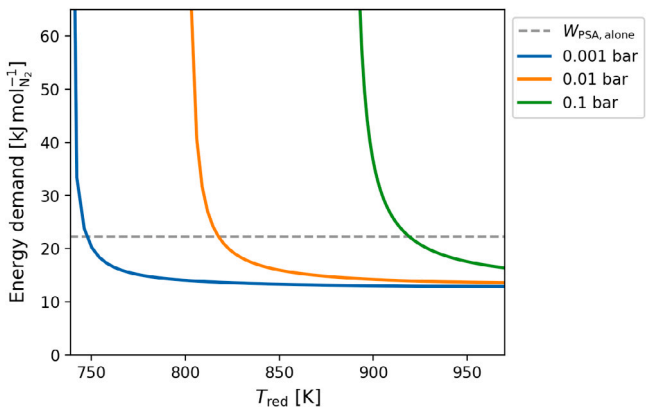

Fig. 7. Total energy demand E_{tot} vs. T_{red} for 3 different values of reduction vacuum pressure p_{red}. Also plotted is the energy demand using PSA alone $W_{PSA,alone}$.

Table 2
The mass dimensions and void fraction of the pellet used in the kinetic study.

Mass	806 [mg]
Diameter	7.9 [mm]
Height	3.8 [mm]
Void fraction ϵ_{pellet}	0.185 [–]

infinity. The work of the vacuum pump W_{vac} decreases with p_{red}, but this appears to be outweighed by the effect of p_{red} on $\Delta\delta$. The results show that a reduction pressure of $p_{red} = 0.1$ bar, would require reduction temperatures exceeding 900 K, which may be impractical for the system. For reduction pressures in the range $p_{red} = 0.01 - 0.001$ bar, a reduction temperature of 873 K is sufficient for the process. This shows that there is flexibility in the thermodynamic limitations to accommodate design optimisation with readily available components.

3. Experimental analysis

With a promising thermodynamic outlook, we can now move on to analysing the process from both a kinetic and durability perspectives. Therefore, in this section we experimentally assess the kinetic reaction rates, and the chemical stability of the material over many cycles.

3.1. Kinetics

The reduction takes place at 873 K, with oxygen directly removed via pumping. Under these conditions the kinetics are very fast [12], and under reasonable operating conditions this step would be limited by the pumping speed rather than intrinsic kinetics. The oxidation kinetics on the other hand take place at lower temperatures and under low oxygen partial pressures, where kinetics will play an important role. A previous kinetic model by the authors focused largely on the oxidation kinetics in pure oxygen [12]. However, for oxygen as a dilute gas in nitrogen the kinetic regime could be quite different due to a more complex mass transfer in the gas phase within and around pellets/granules. Therefore, an isothermal relaxation kinetic study was performed for the oxidation of an $SrFeO_3$ pellet at $T_{ox} = 623$ K, under various oxygen concentrations.

The $SrFeO_3$ was synthesised via a solid state annealing of $SrCO_3$ and Fe_3O_4 powders mixed together, which is described in detail in previous work [4,12]. The resulting $SrFeO_3$ powder was pressed into an 8 mm diameter pellet and annealed at 1573 K for 10 h. The mass and dimensions of the resulting pellet are given in Table 2, which were combined with the density of SF ρ_{SF} 5310.0 kg m^{-3}, to determine the pellet void fraction of ϵ_{pellet}.

For the relaxation study the pellet was first reduced at the conditions proposed in the process; 873 K under a gas flow with an oxygen partial pressure of $p_{O_2} = 0.01$. The pellet was then cooled to 623 K and

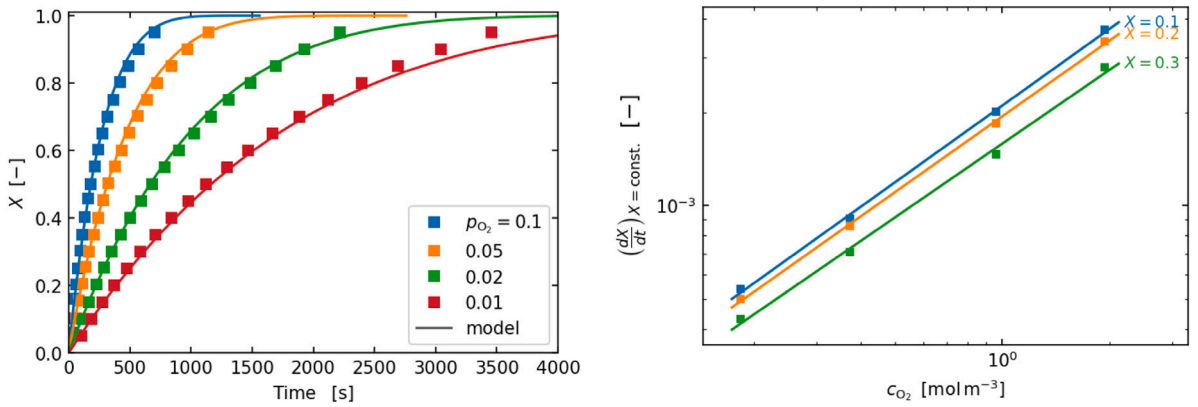

Fig. 8. Left: Extent of reaction X vs. time for the oxidation of the pellet at partial pressures $0.1 - 0.01$ bar, showing experimental data and the model given in Eq. (13). **Right:** A log–log plot of the rate vs. the oxygen concentration for three different conversion extents (X = 0.1, 0.2, and 0.3), showing the linear fits used to determine concentration dependence n.

Table 3
Kinetic model parameters for Eq. (13), determined from the numerical fit of the data shown in Fig. 8.

k	$2.13(1) \times 10^{-3}$	$[(\text{mol m}^{-3})^{-n}\ \text{s}^{-s}]$
n	0.81(1)	[–]
m	0.8(1)	[–]

oxidised under different oxygen partial pressures in the range $1 - 0.01$ bar. To analyse the data we use the same approach as in our previous work [12], but focused on lower partial pressures. Full details of the kinetic study are given in the ESI.

Fig. 8 shows the kinetic data at lower partial pressures of 0.1–0.01 bar, with the reaction extent X, given by,

$$X = \frac{\delta_0 - \delta(t)}{\delta_0 - \delta_{eq}(T, p_{O_2})}, \tag{12}$$

where δ_0 is the non stoichiometry at $t = 0$ and $\delta_{eq}(T, p_{O_2})$ is the equilibrium non-stoichiometry at the given oxygen partial pressure. Data at higher partial pressures was omitted as it showed a different trend in the X dependence, indicating a different reaction regime (see ESI). This rate can be seen to decrease with increasing X with a power law dependence, indicating a kinetic model of the form,

$$\frac{dX}{dt} = kC_{O_2}^{n}(1 - X)^{m}\ [\text{s}^{-1}]. \tag{13}$$

where k is the rate constant at this temperature, n is the power law dependence on oxygen concentration, and m is the power law dependence on reaction extent X. These parameters were determined by making numerical fits of the experimental data and are given in Table 3. It was verified that the kinetics were not limited by the system (heat or mass transfer), and therefore represent kinetic limitations of the pellet itself. To check the performance of a packed bed reactor we can use this kinetic model to represent the oxidation rate of a pellet within the packed bed.

3.2. Chemical looping stability tests

The stability of the $SrFeO_3$ chemical redox reactions was investigated over 250 cycles. A total of 527 mg of the prepared $SrFeO_3$ powder was placed in the TGA and cycled 250 times between a reduction step at 850 K in an oxygen partial pressure $p_{O_2} = 0.01$ bar, and an oxidation step at 630 K in an oxygen partial pressure $p_{O_2} = 0.2$ bar.

The results from these cycling experiments are shown in Fig. 9, where it can be seen that the material's total mass change during each cycle is close to a constant. After 250 cycles there is an approximate decrease in the oxygen stored of 1%, which could be a result of drift in the TGA mass measurements. This high chemical stability is expected, due to the fact that our material was annealed at 1473 K, which is 600 K higher than the temperatures used in the cycle. Furthermore, $SrFeO_3$ undergoes partial reduction, without any major phase changes, so that the lattice remains intact throughout the cycle [9]. Fig. 9 also shows the oxidation step of the 10th and 240th cycle, where both show almost identical profiles. The chemical cycle stability is therefore seen from both a kinetic and total yield perspective.

4. Packed bed reactor model

Next we formulate a model of the packed bed reactors. The reduction takes place at 873 K, with oxygen directly removed via pumping, where the kinetics are very fast [12], and so we assume the reduction goes to equilibrium $\delta_{red} = \delta_{eq}(T_{red}, p_{red})$. We therefore focus our attention more on the oxidation step, where the reaction between oxygen gas at low partial pressures and the solid reactor bed may lead to critical kinetic limitations.

4.1. Packed bed model assumptions

A reactor containing a fixed bed of SF pellets was simulated under the following assumptions:

1. A 1D model along the length of the reactor with radial symmetry of the domain.
2. No gravitational effects.
3. Volume of $SrFeO_3$ pellets are unchanged by the reaction.
4. The process is isothermal with a uniform temperature throughout the packed bed.
5. The pressure drop across the bed is neglected.
6. The kinetics are assumed to follow the model parameters determined in the previous section for the 8 mm diameter pellet.

The first two assumptions are standard simplifications used to model packed bed reactor as one dimensional systems. The third assumption is justified from experimental observations of the $SrFeO_3$ perovskite lattice parameters during reduction, which shows a small <2% change over a broad range of δ [9]. For the fourth assumption we show that the heat capacity of the bed and feed gases is much larger than the heat of reaction, allowing an adiabatic reactor to operate approximately isothermally (see ESI). To justify the fifth assumption, we calculate the pressure drop across a packed bed for the process conditions suggested, and find it to be negligible (see ESI). The sixth assumption is that the kinetics will be in the same regime as what we have measured for our pellet. This kinetic expression includes oxygen transport within the pellet (gas or solid phase transport), so that the pellet's volume will be omitted from the gas phase convection–diffusion domain.

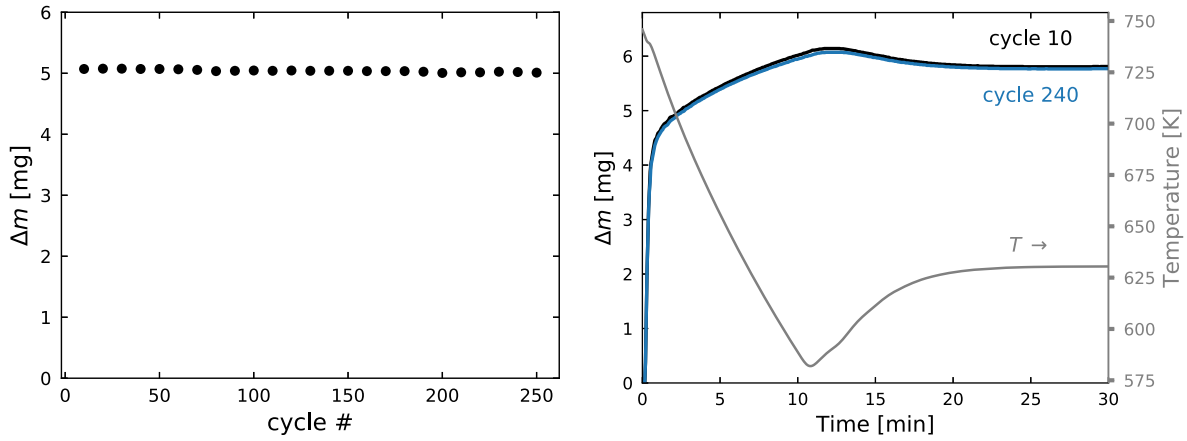

Fig. 9. Left: Total mass change vs. cycle number for every 10th cycle of the $SrFeO_3$. **Right:** The oxidation step of cycle number 10 and cycle number 240 compared.

With these assumptions we can then model the packed reactor with two independent variables; the oxygen concentration C_{O_2} modelled with a convection–diffusion equation in the void space of the packed bed, and the oxide non-stoichiometry in the solid phase δ.

4.2. Model equations

The general convection–diffusion equation for dilute species in porous media with a chemical reaction source term was used to model the gas moving through the packed bed reactor [22],

$$\varepsilon_{bed}\frac{\partial C_{O_2}}{\partial t} = -\frac{\partial (u_s C_{O_2})}{\partial x} + D_{\text{eff}}\frac{\partial^2 C_{O_2}}{\partial x^2} + 0.5 C_{SF}\left(\frac{\partial \delta}{\partial t}\right) \tag{14}$$

where u_s is the superficial velocity, D_{eff} is the effective diffusion coefficient of oxygen in nitrogen [23], and ε_{bed} is the free volume of the reactor (volume not occupied by the pellets/granules). The last term is the chemical reaction source term, which is given by the concentration of SF in the reactor $C_{\text{SF}} = \frac{n_{\text{SF}}}{V_{reactor}}$ multiplied by 0.5 for the stoichiometry of the reaction and the kinetic rate of change of non-stoichiometry, $\frac{\partial \delta}{\partial t}$. The rate of change in δ, $\frac{\partial \delta}{\partial t}$ was calculated using the kinetic model given in Eq. (13) with the parameters given in Table 3, and using the formulae [12],

$$X(t) = \frac{\delta_{\text{red}} - \delta(t)}{\delta_{\text{red}} - \delta_{eq}(p_{O_2}(t), T)}. \tag{15}$$

Here $\delta_{eq}(p_{O_2}(x,t), T_{\text{ox}})$, refers to the equilibrium for the local oxygen concentration $p_{O_2} = \frac{C_{O_2}}{RT}$.

The initial condition throughout the reactor was, for the SF,

$$\delta(t=0) = \delta_{\text{red}}. \tag{16}$$

and for the gas phase, the corresponding equilibrium oxygen concentration for δ_{red} at the oxidation temperature,

$$C_{O_2}(t=0) = C_{O_2,\text{eq}} = \frac{p_{O_2,\text{eq}}(\delta_{\text{red}}, T_{\text{ox}})}{RT}. \tag{17}$$

The reduction extent δ_{red} was determined by assuming we achieve the equilibrium value during this step. For the inlet boundary condition ($x = 0$) we have the concentration of the incoming gas,

$$C_{O_2}(x=0) = C_{O_2,\text{in}} = x_{O_2,\text{PSA}}\frac{p_{\text{ox}}}{RT}. \tag{18}$$

At the outlet of the packed bed $x = L_{\text{bed}}$ we have an outflow condition. We then need to solve this on the domain $x \in [0, L_{\text{bed}}]$, and $t \in [0, 0.5 t_{\text{cycle}}]$.

To get a numerical solution of $C_{O_2}(x,t)$ and $\delta(x,t)$, we used the finite volume method in a 1D space with uniform mesh size of 200 cells. We used the upwind scheme for the convection term and the central difference scheme for the diffusion term. An explicit solution method was implemented, with full details given in Section 4 of the ESI.

Table 4
Parameters for the packed bed simulation for comparison to the experimental results from Bulfin *et al.* [4].

Packed bed operating conditions		
L_{bed}	0.15	[m]
R_{bed}	0.01	[m]
ε_{bed}	0.72	[–]
m_{SF}	0.0482	[kg]
$\dot{v}$ (at 298 K)	219	[sccm]
u_s (at 623 K)	0.0235	[m s^{-1}]
C_{SF}	5406	[mol m^{-3}]
$x_{O_2,\text{in}}$	0.2	[–]
T_{ox}	623	[K]
T_{red}	1073	[K]
p_{ox}	1.01	[bar]
p_{red}	0.025	[bar]

4.3. Model validation

In previous work, Bulfin et al. [4] performed a technology demonstration of this process, where a small packed bed of $SrFeO_3$ granules was rapidly heated and cooled under various flows of synthetic air mixtures. The process was demonstrated for two cases, one for removal of oxygen from undiluted air and one for oxygen removal from "precleaned" air ($\approx 1\%O_2$). In order to validate our packed bed model, we simulate the experiments performed to compare the outlet concentration of oxygen over time. Both oxidations were performed at $T_{\text{ox}} \approx 623$ K, which is the same temperature we have measured our kinetics, so that they should be suitable for validation. Here we show the results of the case for oxygen removal from synthetic air, and in the ESI we show the results for the "precleaned" air.

For the parameters of the packed bed we use the values reported in Bulfin et al. [4] for their packed bed, which are given in Table 4. The granules in the packed bed were taken to have a void space $\varepsilon_{\text{granules}} = 0.3$, and together with the total mass of SF m_{SF} and the volume of the bed $V_{\text{bed}} = \pi L_{\text{bed}} R_{\text{bed}}^2$, this allowed the void space of the bed to be calculated, ε_{bed} (the void space of the bed does not include the void space within the pellets). The superficial velocity was calculated using the gas feed rate and cross sectional area of the reactor tube and the volumetric flow rate at the oxidation temperature $u_s = \frac{\dot{v}}{\pi R_{\text{bed}}^2}$. Finally, the concentration of SF in the bed can be calculated using the bed volume, the mass of SF and the molar mass of SF, $C_{\text{SF}} = \frac{m_{\text{SF}}}{V_{\text{bed}} M_{\text{SF}}}$.

Fig. 10 shows the results of the simulation with a comparison to experimental outlet oxygen concentration vs. time. From the comparison of the outlet oxygen mole fraction we can see that the simulation outperforms the experiment. There could be a number of reasons for

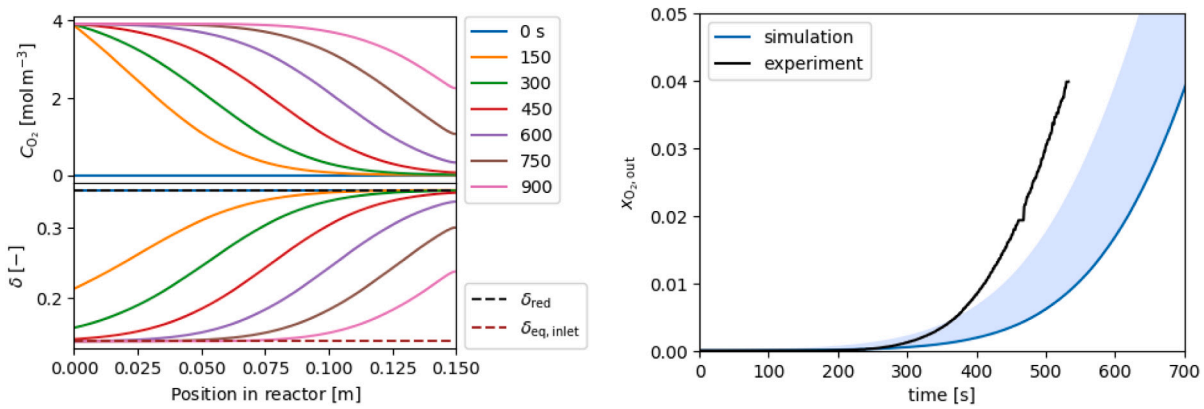

Fig. 10. Simulation of the undiluted air case from the technology demonstration by Bulfin et al. [4] with parameters given in Table 4. **Left:** The oxygen gas concentration c_{O_2}, and the SF non-stoichiometry δ, vs. position x along the reactor at various times throughout the oxidation step. **Right:** Outlet molar fraction $x_{O_2,out}$ plotted against time for the simulation and experiment. The boundary of the shaded region above the simulation shows the model run with a slower kinetic rate using the error reported for the parameter $m = 0.8(1)$, and a lower reduction temperature $T_{red} = 1023$ K.

differences between simulation and experiment. The main reason is likely the fact that the granules in the experiment have diameters $d = 3.5 - 4.5$ [mm] comparable to that of reactor tube $d = 20$ [mm]. In this case edge effects can result in preferential flow paths and would lead to shorter average residence times, as opposed to the uniform flow distribution in our 1D model. In addition, the temperatures in the experiment were measured at the centre of the bed, where the average temperature could be lower leading to slower kinetics, and a lower average reduction extent δ_{red}.

The edge of the shaded region in Fig. 10 shows a model run with lower values for reduction temperature and slower kinetics within the experimental errors of the kinetic study, to highlight the effect these uncertainties can have on the simulations. This region comes much closer to the experimental outflow oxygen mole fraction. Very similar trends are seen for comparison of the model to the pre-cleaned air shown in the ESI, with the model again outperforming the experimental case. However, given the uncertainties faced in modelling this experimental demonstration the agreement in the general trend is relatively good.

In Fig. 10 (left) it can also be seen that at the inlet of the packed bed, the SF reaches equilibrium with the inlet oxygen concentration $\delta = \delta_{eq}(x_{O_2,in} p_{ox}, T_{ox})$, while the SF at the exit remains unoxidised. This means that more oxygen can be absorbed by the bed than in the zero dimensional case used for the energy balance calculations, which assumed the oxide could only be oxidised to equilibrium with the cut-off oxygen pressure, $\delta_{eq}(x_{O_2,cutoff} p_{ox}, T_{ox})$. This is a general performance improvement seen for a plug flow reactor relative to a perfectly mixing reactor [24]. This will lead to better utilisation of the SF bed, and further improve the energy balance of the process.

4.4. Scaled up system

In this section we use the 1D model to simulate a test case system for the production of 1000 N m^3 h^{-1} with a cut off oxygen impurity of $x_{O_2,cutoff} = 3{\cdot}10^{-6}$. All parameters for this test case are given in Table 4. We assume the PSA system is used to pre-clean the air to $x_{O_2,PSA} = 0.001$, which could for example be achieved with the Genron system shown in Fig. 1. This level of purification in the PSA system allows for a smaller add on redox unit to achieve high purity, while maintaining a relatively high capacity for the PSA system.

We model a packed bed of pellets assumed to be identical to those manufactured for the kinetic analysis with dimensions given in Table 2. The maximum random packing density of cylinders with this aspect ratio is approximately 0.68 [25]. A loosely packed bed would fall short of this maximum, and so we have selected a bed with a packing density of 0.6, giving a bed void fraction of $\epsilon_{bed} = 0.4$.

Table 5
Parameters for the packed bed simulation for comparison to the experimental results from Bulfin *et al.* [4].

Packed bed design parameters		
L_{bed}	0.5	[m]
R_{bed}	0.5	[m]
ϵ_{bed}	0.4	[–]
m_{SF}	855	[kg]
$\dot{v}$ (at 298 K)	1000	[N m^3 h^{-1}]
u_s (at 623 K)	0.041	[m s^{-1}]
C_{SF}	13 677.0	[mol m^{-3}]
$x_{O_2,in} = x_{O_2,PSA}$	0.001	[–]
T_{ox}	623	[K]
T_{red}	873	[K]
p_{ox}	20	[bar]
p_{red}	0.005	[bar]
$x_{O_2,cutoff}$	$3 \cdot 10^{-6}$	[–]
$t_{cycle} = 2t_{cutoff}$	12.8	[h]

The packed beds were then scaled so that they will have a relatively long cycle time of approximately 12 h, with size parameters given in Table 3. The long cycle time will allow a generous six hours for the regeneration of the packed beds in the reduction step, via heating and vacuum pumping. The diameter of the bed was set to allow for a relatively low superficial velocity of approximately 4 cm s^{-1}. We assumed that the compressor was used to increase the pressure to 20 bar, which also reduces the flow velocity and increases the partial pressure of oxygen in the incoming flow.

The results for an oxidation cycle of the packed bed simulated using our 1D reactor model are shown in Fig. 11. If each pellet does have oxidation kinetics in-line with our kinetic measurements, this bed would be suitable for over six hours of oxidation time before reaching the cut-off oxygen mole fraction. With two beds this would give over 12 h for a single cycle. However, it is important to discuss the assumption that the oxidation kinetics will be the same as in our experimental tests. We do have the same temperature $T_{ox} = 623$ K, and similar oxygen partial pressures at the input $p_{O_2,in=0.02\,bar}$, but we also have a larger total pressure $p_{ox} = 20$ bar. This change in total pressure can affect the kinetics because the gas phase diffusion coefficient scales with the inverse of the pressure, $D_{O_2} \propto \frac{1}{p}$. However, the pellets were relatively large, and dense (18% void space), so that it is unlikely that gas phase diffusion within the pellet is playing the limiting role, or we might expect almost negligible oxidation rates. A previous kinetic study at even lower temperatures, showed rapid oxidation kinetics, which indicates a high solid phase diffusion rate [12]. Therefore, we are assuming that the solid phase diffusion of oxygen ions is responsible for the transport of oxygen within the pellet. If this is valid then the

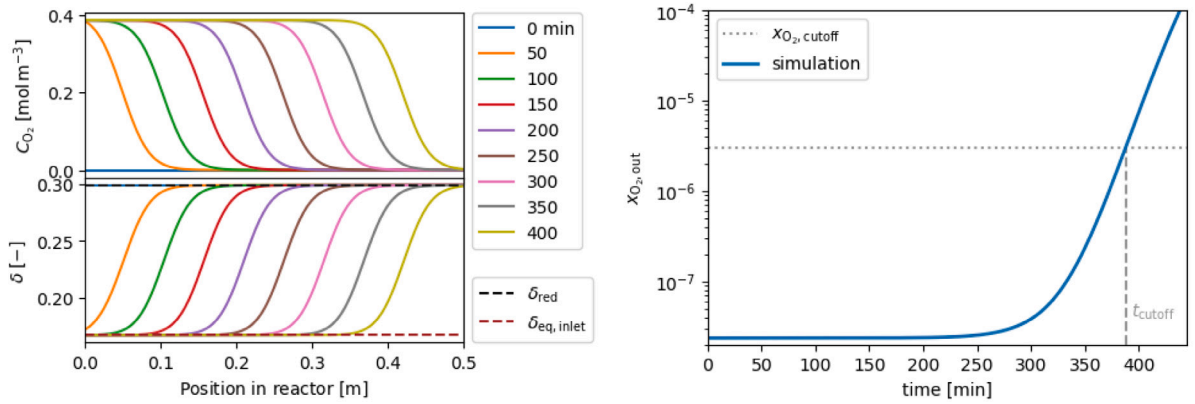

Fig. 11. Simulation of a packed bed for use in a 1000 N m^3 h^{-1} nitrogen processes as illustrated in Fig. 2 with process parameters given in Table 5. **Left:** The oxygen gas concentration c_{O_2}, and the SF non-stoichiometry δ, vs. position x along the reactor at various time throughout the oxidation step. **Right:** The mole fraction of oxygen in the output stream $x_{O_{2,out}}$ vs. time, with the cut-off mole fraction $x_{O_{2,cutoff}}$, and the time taken to reach this value t_{cutoff}, also shown.

Table 6
Oxygen storage capacity $\Delta\delta$ for the thermodynamic model, the 1D model maximum and the average value over the packed bed at the cut-off time for the data plotted in Fig. 11.

	δ_{ox}	$\Delta\delta$
Thermodynamic model	$\delta_{eq}(T_{ox}, x_{O_2,cutoff} p_{ox})$	0.06
1D model max	$\delta_{eq}(T_{ox}, x_{O_2,in} p_{ox})$	0.131
Simulation	$\bar{\delta}$	0.107

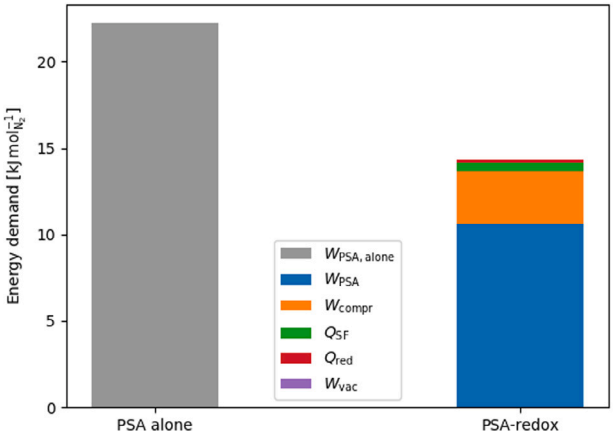

Fig. 12. Energy demand of nitrogen production using a PSA alone $W_{PSA,alone}$, and on the right the energy demand using a combined PSA-redox process $E_{tot} = W_{PSA} + W_{compr} + Q_{SF} + Q_{red} + W_{vac}$, which was calculated using the mass balance of the test case simulation shown in Fig. 11 and following the methodology from the thermodynamic model section. In this case $Q_{gas} = 0$, due to the heat provided by the compressor.

modelled reactor should be relatively accurate. Further experimental tests at larger pressures would be required to validate this assumption.

As mentioned in the previous section, the flow configuration of the packed bed allows the SF to be oxidised beyond what was assumed in the thermodynamic model. This is summarised in Table 6, where it can be seen that the packed bed simulated here has 80% higher oxygen storage than was assumed in the thermodynamic energy balance calculations. We can make an energy balance for this specific case using the same methodology as the thermodynamic model but using the larger $\Delta\delta$ found in the simulation.

In Fig. 12 it can be seen that the energy demand calculated for this test case is lower than for the PSA system alone. The energy demand of the combined PSA-redox process is largely made up of the work of the PSA, followed by the work of the compressor. The energy to heat SF Q_{SF}, is relatively small in this case because the pre-cleaning was to 0.1% oxygen, and the larger oxygen storage $\Delta\delta$ relative to the thermodynamic model, both of which lead to less SF required to be cycled per mole of nitrogen produced.

In addition to the improved energy balance, this process design also allows a given PSA system to maintain a high production capacity, due to the lower purity leaving the PSA. When considering the cost of producing high purity nitrogen at intermediate scale this could improve both capital and operating expenditure, as we reduce the energy demand and increase the capacity of a given PSA system.

5. Conclusions

This work highlights the high potential for application of a chemical looping redox process based on $SrFeO_3$, for the removal of residual oxygen coming from a PSA system. It could allow for competitive production of nitrogen at intermediate scales and high purity. The thermodynamic analysis presented here showed an approximate energy demand of 14 kJ mol$^{-1}_{N_2}$ for a cut-off oxygen impurity of 3×10^{-6}. The kinetic analysis combined with the modelling of the packed bed, also showed very promising performance for oxygen removal. Cycle stability tests showed reversible oxygen storage at the relevant process conditions over 250 cycles. Overall, the study indicates that this nitrogen production process could be very interesting for industrial application.

Declaration of competing interest

The authors declare that they have no known competing financial interests or personal relationships that could have appeared to influence the work reported in this paper.

Acknowledgments

This work was funded in part by the Swiss Federal Office of Energy, Switzerland (Grant No. SI/501213-01) and the European Union's Horizon 2020 Research Infrastructure Programme (Project SFERA-III – Grant Nr. 823802).

Appendix A. Supplementary data

Supplementary material related to this article can be found online at https://doi.org/10.1016/j.cej.2020.127734.

References

[1] J.W. Erisman, M.A. Sutton, J. Galloway, Z. Klimont, W. Winiwarter, How a century of ammonia synthesis changed the world, Nat. Geosci. 1 (10) (2008) 636–639.

[2] R. Thorogood, Developments in air separation, Gas Sep. Purif. 5 (2) (1991) 83–94.

[3] A. Schulte-Schulze-Berndt, K. Krabiell, Nitrogen generation by pressure swing adsorption based on carbon molecular sieves, Gas Sep. Purif. 7 (4) (1993) 253–257.

[4] B. Bulfin, J. Lapp, S. Richter, D. Gubàn, J. Vieten, S. Brendelberger, M. Roeb, C. Sattler, Air separation and selective oxygen pumping via temperature and pressure swing oxygen adsorption using a redox cycle of $SrFeO_3$ perovskite, Chem. Eng. Sci. 203 (2019) 68–75, http://dx.doi.org/10.1016/j.ces.2019.03.057, URL http://www.sciencedirect.com/science/article/pii/S0009250919303306.

[5] H. Ikeda, S. Nikata, E. Hirakawa, A. Tsuchida, N. Miura, Oxygen sorption/desorption behavior and crystal structural change for $SrFeO_{3-\delta}$, Chem. Eng. Sci. 147 (2016) 166–172.

[6] A. Holt, T. Norby, R. Glenne, Defects and transport in $SrFe_{1-x}Co_xO_{3-\delta}$, Ionics 5 (5–6) (1999) 434–443.

[7] H.E. Bush, R. Datta, P.G. Loutzenhiser, Aluminum-doped strontium ferrites for a two-step solar thermochemical air separation cycle: Thermodynamic characterization and cycle analysis, Sol. Energy 188 (2019) 775–786.

[8] K. Krishnamurthy, D. Acharya, F. Fitch, Pilot-Scale Demonstration of a Novel, Low-Cost Oxygen Supply Process and its Integration with Oxy-Fuel Coal-Fired Boilers, Tech. rep., Boc Group, Inc., The (A Delaware Corp), 2008.

[9] J. Vieten, B. Bulfin, F. Call, M. Lange, M. Schmücker, A. Francke, M. Roeb, C. Sattler, Perovskite oxides for application in thermochemical air separation and oxygen storage, J. Mater. Chem. A 4 (35) (2016) 13652–13659.

[10] M. Ezbiri, K.M. Allen, M.E. Gàlvez, R. Michalsky, A. Steinfeld, Design principles of perovskites for thermochemical oxygen separation, ChemSusChem 8 (11) (2015) 1966–1971.

[11] M. Ezbiri, A. Reinhart, B. Huber, K. Allen, A. Steinfeld, B. Bulfin, R. Michalsky, High redox performance of $Y_{0.5}Ba_{0.5}CoO_{3-\delta}$ for thermochemical oxygen production and separation, React. Chem. Eng. 5 (4) (2020) 685–695.

[12] B. Bulfin, J. Vieten, S. Richter, J. Naik, G. Patzke, M. Roeb, C. Sattler, A. Steinfeld, Isothermal relaxation kinetics for the reduction and oxidation of $SrFeO_3$ based perovskites, Phys. Chem. Chem. Phys. 22 (4) (2020) 2466–2474.

[13] F.G. Kerry, Industrial Gas Handbook: Gas Separation and Purification, CRC press, 2007.

[14] I. Starkov, S. Bychkov, A. Matvienko, A. Nemudry, Oxygen release technique as a method for the determination of "δ-p_{O_2}-T" diagrams for miec oxides, Phys. Chem. Chem. Phys. 16 (12) (2014) 5527–5535.

[15] M. Patrakeev, J. Shilova, E. Mitberg, A. Lakhtin, I. Leonidov, V. Kozhevnikov, Oxygen intercalation in strontium ferrite: Evolution of thermodynamics and electron transport properties, in: New Trends in Intercalation Compounds for Energy Storage, Springer, 2002, pp. 565–572.

[16] V. Vashuk, L. Kokhanovskii, I. Yushkevich, Electrical conductivity and oxygen stoichiometry of $SrFeO_{3-\delta}$, Inorg. Mater. 36 (1) (2000) 79–83.

[17] V. Sereda, A. Sednev, D. Tsvetkov, A. Zuev, Enthalpy increments and redox thermodynamics of $SrFeO_{3-\delta}$, J. Mater. Res. 34 (19) (2019) 3288–3295.

[18] J. Vieten, B. Bulfin, P. Huck, M. Horton, D. Guban, L. Zhu, Y. Lu, K.A. Persson, M. Roeb, C. Sattler, Materials design of perovskite solid solutions for thermochemical applications, Energy Environ. Sci. 12 (4) (2019) 1369–1384.

[19] P.T. Krenzke, J.H. Davidson, On the efficiency of solar H2 and CO production via the thermochemical cerium oxide redox cycle: the option of inert-swept reduction, Energy Fuels 29 (2) (2015) 1045–1054.

[20] D.G. Goodwin, R.L. Speth, H.K. Moffat, B.W. Weber, Cantera: An object-oriented software toolkit for chemical kinetics, thermodynamics, and transport processes, 2018, http://dx.doi.org/10.5281/zenodo.1174508, https://www.cantera.org, version 2.4.0.

[21] S. Brendelberger, H. von Storch, B. Bulfin, C. Sattler, Vacuum pumping options for application in solar thermochemical redox cycles–assessment of mechanical-, jet-and thermochemical pumping systems, Sol. Energy 141 (2017) 91–102.

[22] M. Wild, A. Steinfeld, Modelling of a high-temperature thermochemical storage reactor with radial flow across a annular packed bed using the $CaCO_3$-CaO cycle as a model reaction, Proceedings, IEA SHC International Conference on Solar Heating and Cooling for Buildings and Industry (2019) URL http://proceedings.ises.org/paper/swc2019/swc2019-0118-Wild.pdf.

[23] N. Epstein, On tortuosity and the tortuosity factor in flow and diffusion through porous media, Chem. Eng. Sci. 44 (3) (1989) 777–779, http://dx.doi.org/10.1016/0009-2509(89)85053-5, URL http://www.sciencedirect.com/science/article/pii/0009250989850535.

[24] O. Levenspiel, Chemical Reaction Engineering, Wiley Eastern Limited, 1972.

[25] S. Li, J. Zhao, P. Lu, Y. Xie, Maximum packing densities of basic 3D objects, Chin. Sci. Bull. 55 (2) (2010) 114–119.